INTERNATIONAL JOURNAL OF HYDROGEN ENERGY ▮ (▮▮▮▮) ▮▮▮–▮▮▮

Available at www.sciencedirect.com

ScienceDirect

journal homepage: www.elsevier.com/locate/ijhydene

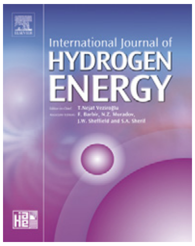

Advanced PVD protective coatings for SOFC interconnects

Paul Gannon[a,*], *Max Deibert*[a], *Preston White*[a], *Richard Smith*[a], *Hui Chen*[a], *Weerashinge Priyantha*[a], *Jake Lucas*[a], *Vladimir Gorokhovsky*[b]

[a]*Montana State University, Bozeman, MT 59717-3920, USA*
[b]*Arcomac Surface Engineering, LLC, Bozeman, MT, USA*

ARTICLE INFO

Article history:
Received 18 June 2007
Received in revised form
4 December 2007
Accepted 5 December 2007

Keywords:
SOFC
PVD
Filtered arc
Protective coatings

ABSTRACT

In an effort to enable inexpensive ferritic steels as interconnects (bi-polar plates) in planar solid oxide fuel cell (SOFC) stacks, advanced large area filtered arc physical vapor deposition (LAFAD) of MCrAlYO ceramic protective coatings was investigated (M = Ti, Co and/or Mn). This manuscript presents three unique LAFAD MCrAlYO coatings, which were applied to 430 ferritic steel specimens and subjected to various SOFC relevant exposures. The coatings' microstructure, composition, area specific resistance (ASR) and Cr volatility were evaluated as a function of exposure to 800 °C air for up to 1000 h. Significant improvement in simulated SOFC interconnect performance was observed with coated vs. uncoated specimens (e.g., increased thermal stability and decreased ASR and Cr volatility). Outward Mn transport (from steel substrate) was observed (to varying extents) in all coatings. This appeared to promote surface crystallization and lower ASR values with extended exposure time. Coatings containing Mn and/or Co as-deposited exhibited the lowest and most stable ASR values, and more-uniform surface crystallization compared with coatings without. Coatings without Mn and/or Co as-deposited retained an amorphous surface structure, apart from local regions of high Mn outward transport, which evolved surface crystallites concentrated at topological features on the substrate steel surface (e.g., roll marks). ASR values for these coatings decreased significantly with exposure time. The engineering of LAFAD MCrAlYO coating processes to enhance SOFC interconnect performance of ferritic steels is presented and discussed.

1. Introduction

Solid oxide fuel cells (SOFCs) are increasingly promising candidates for stationary and portable energy conversion due to their high power density and efficiency, and decreased environmentally sensitive emissions. Typical planar SOFC designs and operation requirements are detailed elsewhere [1–3]. Low cost, ferritic stainless steels (FSSs) are often used as interconnect components (ICs), which physically support and electrically connect individual SOFCs into a modular stack. SOFC-ICs also manifold fuel, oxidant and exhaust gases in and out of respective anode and cathode chambers. In many designs, SOFC-ICs realize simultaneous dual atmosphere (wet reducing and oxidizing) exposures at temperatures up to ~800 °C. To achieve cost competitiveness, SOFC systems must endure several hundred ambient to operating temperature (~800 °C) thermal cycles throughout an over 40,000 h (~4.5 year) life-time [4].

During operation, FSS SOFC-ICs form protective thermally grown oxide (TGO) surface layers, especially in contact with the cathode gas phase (e.g., moist air). Research has focused on both conventional (e.g., 430/441) and specialty (e.g., Crofer

---

[*] *Corresponding author.* Tel.: +406 994 7380.
E-mail address: pgannon@coe.montana.edu (P. Gannon).

0360-3199/$ - see front matter © 2008 International Association for Hydrogen Energy. Published by Elsevier Ltd. All rights reserved.
doi:10.1016/j.ijhydene.2007.12.009

22APU) FSSs during SOFC-IC exposures. These FSS compositions are often observed to evolve duplex TGO surface layers, comprised a fine-grained Cr_2O_3 base layer and a relatively large-grained $(Mn,Cr)_3O_4$ surface layer. After SOFC-IC exposures over thousands of hours, the duplex TGO layers on FSSs often grow to $>10\,\mu m$ (dominated by the Cr_2O_3 base layer), and can exhibit localized exfoliation due to energy release from residual stresses built up within the TGO layers [5]. Continued duplex TGO layer growth and formation of insulating oxides (e.g., SiO_2) also introduce increased contact resistance with adjoining electrodes (measured as area specific resistance (ASR)) [6]. In addition, Cr-transport (from TGO layers in either or both solid and gas phases) into cathodes and cathode/electrolyte interfaces has been cited in SOFC stack performance degradation [7–10].

To improve SOFC-IC performance of FSSs, various surface coating technologies are under research and development. The functional requirements for protective coatings on FSSs for the SOFC-IC application are multifold, e.g., they must: (1) serve as a barrier against inward transport of oxidizing species and outward transport of Cr-containing species (both gas and solid phases); (2) retain low ASR ($<100\,m\Omega\,cm^2$); and (3) exhibit thermal–mechanical and chemical compatibility with adjoining stack components (e.g., no deleterious reactions with electrode or seal materials). Combined satisfaction of the above requirements must be achieved to the extent that SOFC stack voltage degradation is less than 0.1% per 1000 h throughout the desired SOFC system life-time. In addition, SOFC-IC materials must be amenable to high-throughput (and low cost) production to meet anticipated market demands, e.g., 700 MW/year planar SOFC module production at ~70 W/SOFC would require the production of ~10,000,000 ICs/year.

The present work is focused upon enhancement of commercially available FSS 430 using surface coatings from large area filtered arc deposition (LAFAD) developed at Arcomac Surface Engineering, LLC [11]. Related studies are abundant, with a variety of coating deposition techniques being investigated to establish conductive perovskite and spinel oxides on different FSSs. More promising coating compositions from these related studies include various doped lanthanum chromite and manganite perovskites, e.g., $La_{1-x}Ca_xCrO_3$ and $La_{1-x}Sr_xMnO_3$, and various Co-, Fe-, Ni-, Cu- and/or Mn-containing spinels, e.g., $(Co,Mn)_3O_4$ and $(Cu,Mn)_3O_4$ deposited by a range of solution and vapor-based approaches including thermal or plasma spray, slurry coating and physical or chemical vapor deposition [12–17]. In this paper, three unique LAFAD thin film ($<5\,\mu m$) coatings from the TiCoMnCrAlYO elemental system are investigated with the aim of enhanced understanding of the influences of coating composition and architecture on long-term stability during SOFC-IC exposures.

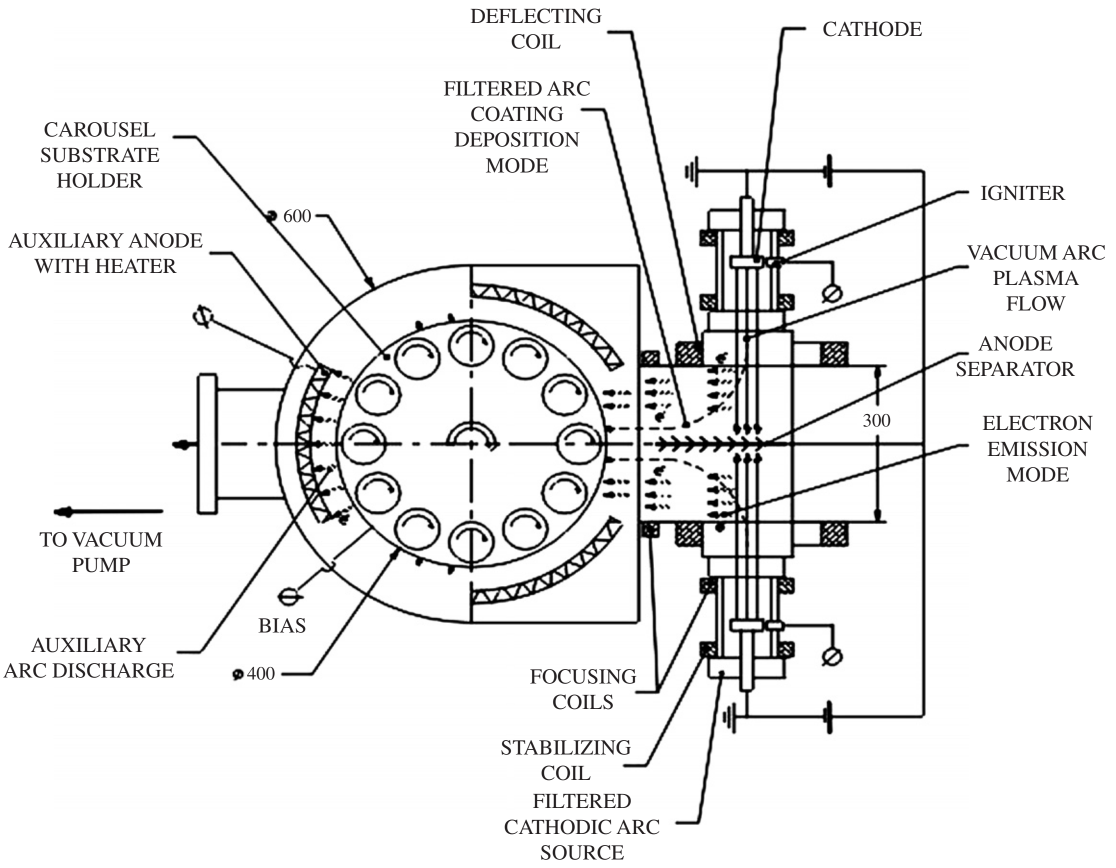

Fig. 1 – Schematic of LAFAD surface engineering system (plan view).

Please cite this article as: Gannon P, et al. Advanced PVD protective coatings for SOFC interconnects. Int J Hydrogen Energy (2008), doi:10.1016/j.ijhydene.2007.12.009

2. Experimental

2.1. *Coating processes*

LAFAD coatings were deposited on sheets (100 × 100 × 1 mm^3) of FSS 430 (acquired from Alleghany Ludlum). Details of the LAFAD coating process parameters and basic coating characteristics are provided elsewhere [12]. Presented here are results from three unique LAFAD processes, producing thin-film ($<5\,\mu$m) coatings with different chemical compositions and thicknesses. For reference, a simplified schematic of the LAFAD system is shown in Fig. 1 [12]. Two metal alloy cathode arc targets oppose each other on a chamber wall-mounted dual large area filtered arc source. The target alloy combinations used for the three coatings presented here are shown in Table 1. Target alloy compositions were as follows (in at%): CoMn = 50Co/50Mn, CrAlY = 46Cr/51Al/3Y, CoCrAlY = 30Co/20Cr/47Al/3Y and TiCrAlY = 30Ti/20Cr/47Al/3Y.

Table 1 – LAFAD process matrix and coating reference; lower case letters within the cells are used to reference the three coatings in this paper (ranked according to subsequently measured ASR values, highest to lowest: α, β and γ)

Coatings deposited in reactive O_2 gas	LAFAD target 2	
	CoCrAlY	TiCrAlY
LAFAD target 1		γ
CoMn		
CrAlY	β	α

Prior to coating, specimen tabs of specific geometries for various SOFC-IC relevant exposure tests were cut with an N_2 laser (JE Soares, Inc.—Belgrade, MT). Fig. 2 presents photographs of typical coated and uncoated FSS 430 substrate sheets (100 × 100 × 1 mm^3) showing laser cut specimens (2.5 cm dia. circles, 1 × 2 cm^2 rectangles and 0.5 cm squares) attached via ~1 mm connection tabs. The optical interference observed on the coated sheet (right in Fig. 2) indicates vertical coating thickness variations from the middle (thickest) to the top and bottom margins. Vertical coating thickness variations result from disabling the scanning magnetic field coil within the LAFAD system, and are used to investigate coating behavior vs. thickness. The coatings presented in this study are from the middle rows (second and third rows from top) of the FSS 430 substrate sheet (Fig. 2).

2.2. *Coating properties characterization*

Coating thickness was determined using the CALOtest™ spherical abrasion technique and optimal microscopy, with an accuracy of ±0.1 μm. Coating adhesion was assessed by means of the Mercedes indentation test using a Rockwell C indenter with ~100 N load [18]. Oxidation of the specimen tabs (in 800 °C air) was carried out using a standard furnace operated without control of humidity or air circulation (Bozeman, MT ambient). ASR measurements were made as a function of time in 800 °C air using two identical specimens faced opposite to each other with porous Pt paste contact in standard 4-point probe geometry [19]. Prior to ASR measurements, both uncoated and coated FSS 430 specimens were pre-oxidized in air at 800 °C for 100 h. Subsequent to varying exposure times, sample cross-sections for microscopic analysis were prepared by epoxy-mounting, sectioning and polishing. SEM/energy dispersive X-ray spectroscopy (EDS)

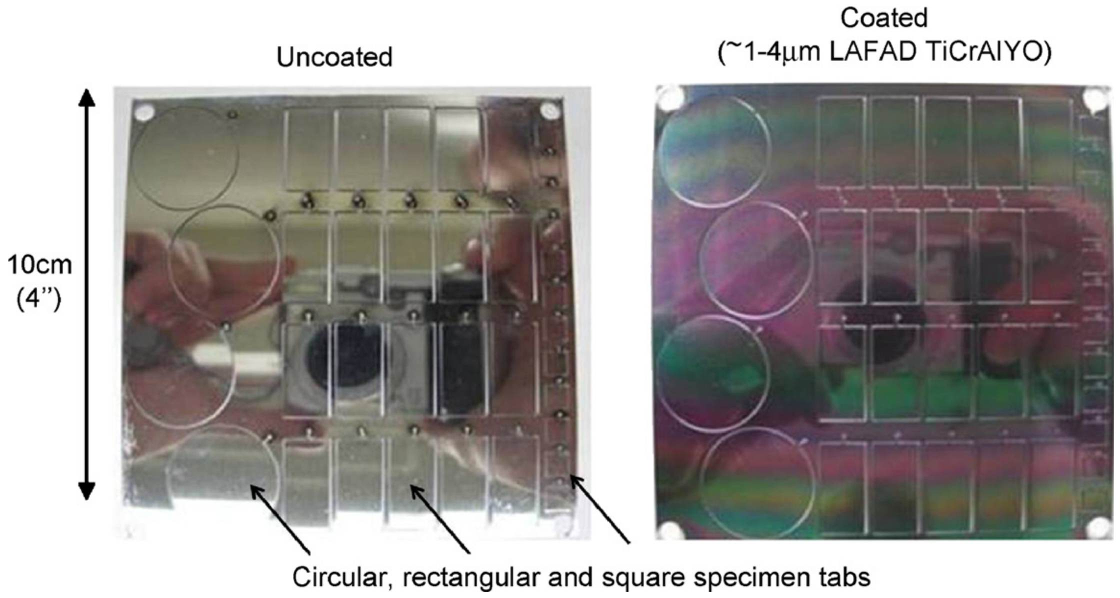

Fig. 2 – Uncoated and LAFAD coated FSS 430 substrate sheets (with laser cut specimens—2.5 cm dia. circles, 1 × 2 cm^2 rectangles and 0.5 cm squares with 1 mm connector tabs).

Please cite this article as: Gannon P, et al. Advanced PVD protective coatings for SOFC interconnects. Int J Hydrogen Energy (2008), doi:10.1016/j.ijhydene.2007.12.009

analysis was performed using a field emission Zeiss Supra VP55 equipped with PGT EDS and HKL backscattered electron diffraction (EBSD) sub-systems. XRD was performed using a Scintag system with thin film detector attachment. Cr volatility was investigated using a novel transpiration apparatus developed at Montana State University [20]. Rutherford backscattering spectroscopy (RBS) analysis of the Si-collection wafer (used in MSU's Cr transpiration apparatus) was performed using a 2 MV van de Graaff accelerator. Composition profiles were determined by comparing SIMNRA computer simulations of spectra with measured data [20]. TERRA thermochemical modeling was employed to facilitate interpretation of the observed Cr volatility from the coated FSS 430 specimen [21].

Table 2 – As-deposited LAFAD coating characteristics

Coating—LAFAD targets	Thickness ranges (µm)	Approximate composition (at%) all have <1%Y; balance O
α-CrAlY/TiCrAlY	~1–4	23Al–14Cr–3Ti
β-CrAlY/CoCrAlY	~0.5–2	18Al–14Cr–12Co
γ-CoMn/TiCrAlY	~0.5–1.5	12Mn–10Al–9Cr–3Ti–<1Co

3. Results and discussion

Results are presented and discussed in the following order: coating compositions and thermal stability; ASR measurements and Cr-volatility measurements.

3.1. *Coating compositions and thermal stability*

Details for the coating matrix presented here (as-deposited) are provided in Table 2. Elemental compositions are from EDS, and are considered a measure of the bulk coating composition. Selected results from each of the three coatings are presented to emphasize common observations throughout extensive analyses on these and similar LAFAD coatings on FSSs.

The high-temperature behavior of coating α (Tables 1 and 2) with different thicknesses is presented in Fig. 3. As deposited, coating α is a complex, weakly crystallized/amorphous TiCrAlY oxide (no discernable XRD peaks) with excellent adhesion to FSS 430 [12]. The froth-like (amorphous) surface structure of the thicker (~4 µm) coating α is not changed significantly from its as-deposited appearance after 1000 h in 800 °C air. This is attributed to the high transport barrier capacity and thermal stability of the amorphous LAFAD TiCrAlY oxide coating. The thinner (~2 µm) coating α exhibits

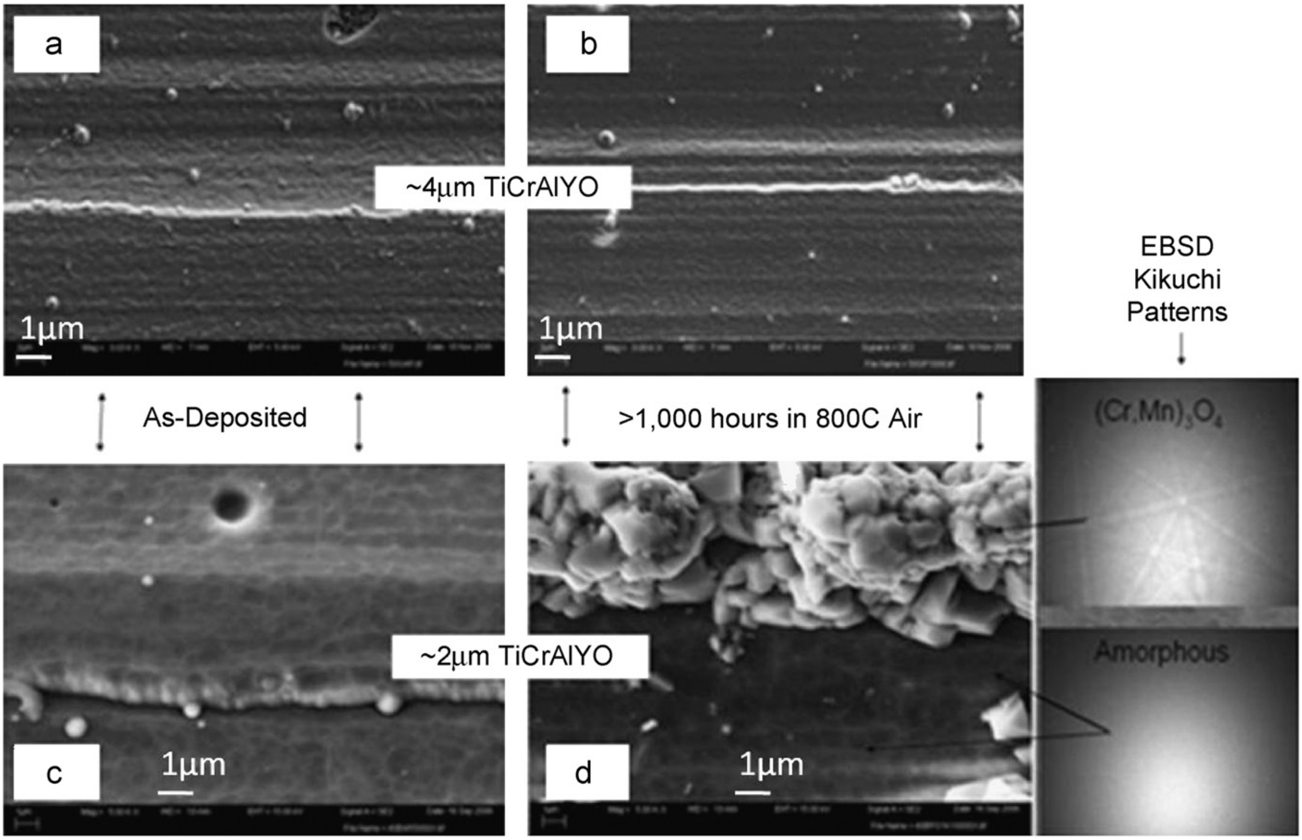

Fig. 3 – SEM surface images and selected area EBSD Kicutchi patterns for coating α before and after 1000 h in 800 °C air (coating thicknesses shown).

Please cite this article as: Gannon P, et al. Advanced PVD protective coatings for SOFC interconnects. Int J Hydrogen Energy (2008), doi:10.1016/j.ijhydene.2007.12.009

areas of relatively unchanged amorphous surface structure and localized surface crystallites, identified as $(Mn,Cr)_3O_4$ spinel by SEM/EDS and selected area EBSD. After the 1000 h, 800 °C air exposure, high oxygen affinity Mn-species have effectively transported from the FSS 430 through the ~2 μm coating α to the surface to form $(Mn,Cr)_3O_4$ spinel surface crystallites. This phenomenon is more pronounced in the thinner coatings, and is preferential along topological features of the FSS 430 surface (e.g., roll marks from sheet processing). Outward Mn transport pathways appear localized at regions of the FSS 430 surface with high-curvature (e.g., terraces, roll marks, etc.). This is evidenced in Fig. 4, which presents via cross-section SEM images of coating α before (Fig. 4a) and after (Fig. 4b,c) the 1000 h exposure. This indicates an influence of substrate surface topology on coating high-temperature behavior, where regions of high-curvature (roughness) perhaps promote defect agglomeration (cation vacancies, quasi-grain boundaries) and create outward Mn diffusion-pathways within the coating. The EDS linescan (Fig. 4c) reveals the presence of Mn throughout coating α, which did not have Mn as-deposited (Table 2). This may help explain the observed decrease in ASR values with time, as presented and discussed later.

As deposited, coating β (Tables 1 and 2) is also a complex, weakly crystallized/amorphous oxide (exhibiting one weak XRD peak tentatively matching $CoCr_2O_4$ spinel) and exhibits excellent adhesion to FSS 430 [12]. In contrast with coating α, coating β contains Co and no Ti (as-deposited). Fig. 5 presents SEM images of coating β's surface before and after 1000 h in 800 °C air. The surface has entirely recrystallized during the exposure, forming complex Mn, Co, Cr and Al-containing isomorphic spinel crystallites, e.g. $(Mn,Co,Cr,Al)_3O_4$. Uniform Mn concentrations are observed over the entire coating surface, indicating coating β permits ubiquitous outward Mn transport from the FSS 430, and not just localized at topological features. Coating β also evolved a compositional stratigraphy during the 1000 h exposure, as shown in the SEM cross-section with EDS elemental line scan in Fig. 6. Interestingly, measured Cr concentrations decrease toward the coating surface, which is elevated in Mn, Co and Al. This particular coating β was ~2 μm thick as-deposited, and thickened to ~3 μm after the 1000 h exposure. This minimal thickening is attributed to the substantially decreased transport of oxidizing species, especially compared with that of the TGO layers on uncoated FSS 430, which can grow to >10 μm during similar exposures.

Fig. 7 presents surface SEM images and XRD patterns for a ~1.5 μm coating γ (Tables 1 and 2) before and after >1000 h in 800 °C air. As deposited, the major peaks observed in the XRD pattern are attributed to the ferritic steel substrate, whereas

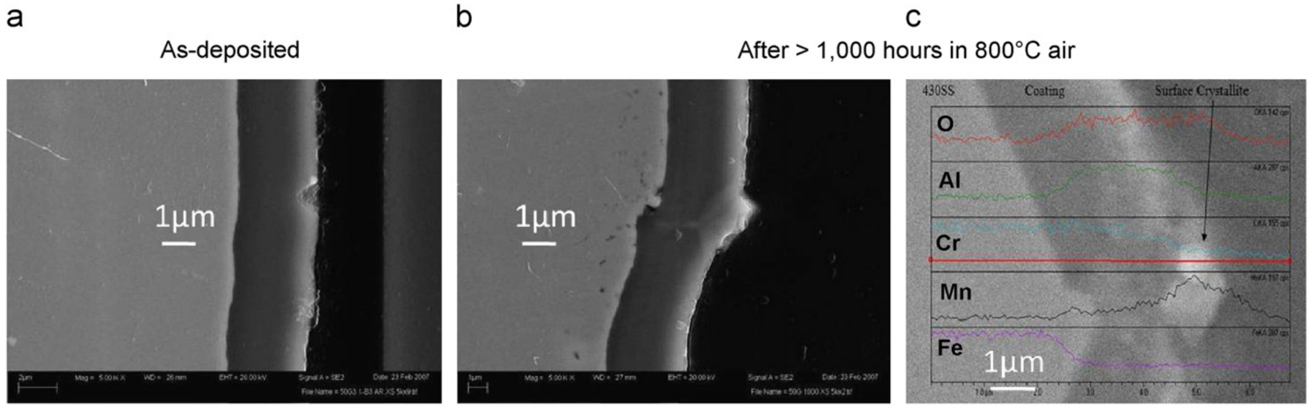

Fig. 4 – SEM cross-section images of coating α before (a) and after (b) 1000 h in 800 °C air; (c) presents an EDS elemental linescan after the exposure.

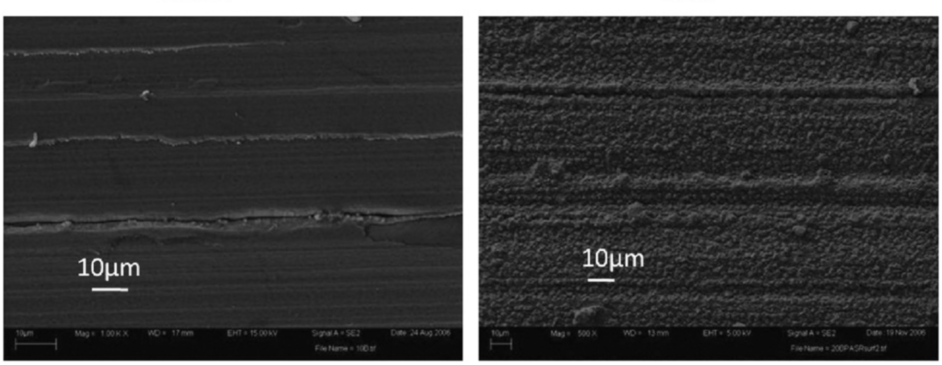

Fig. 5 – SEM surface images of coating β before and after 1000 h in 800 °C air.

Please cite this article as: Gannon P, et al. Advanced PVD protective coatings for SOFC interconnects. Int J Hydrogen Energy (2008), doi:10.1016/j.ijhydene.2007.12.009

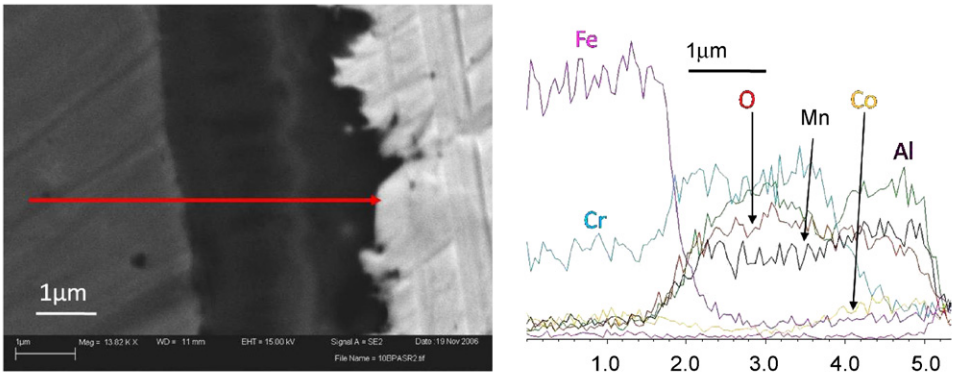

Fig. 6 – Cross-section SEM image and EDS elemental linescan of coating *β* after 1000 h in 800 °C air.

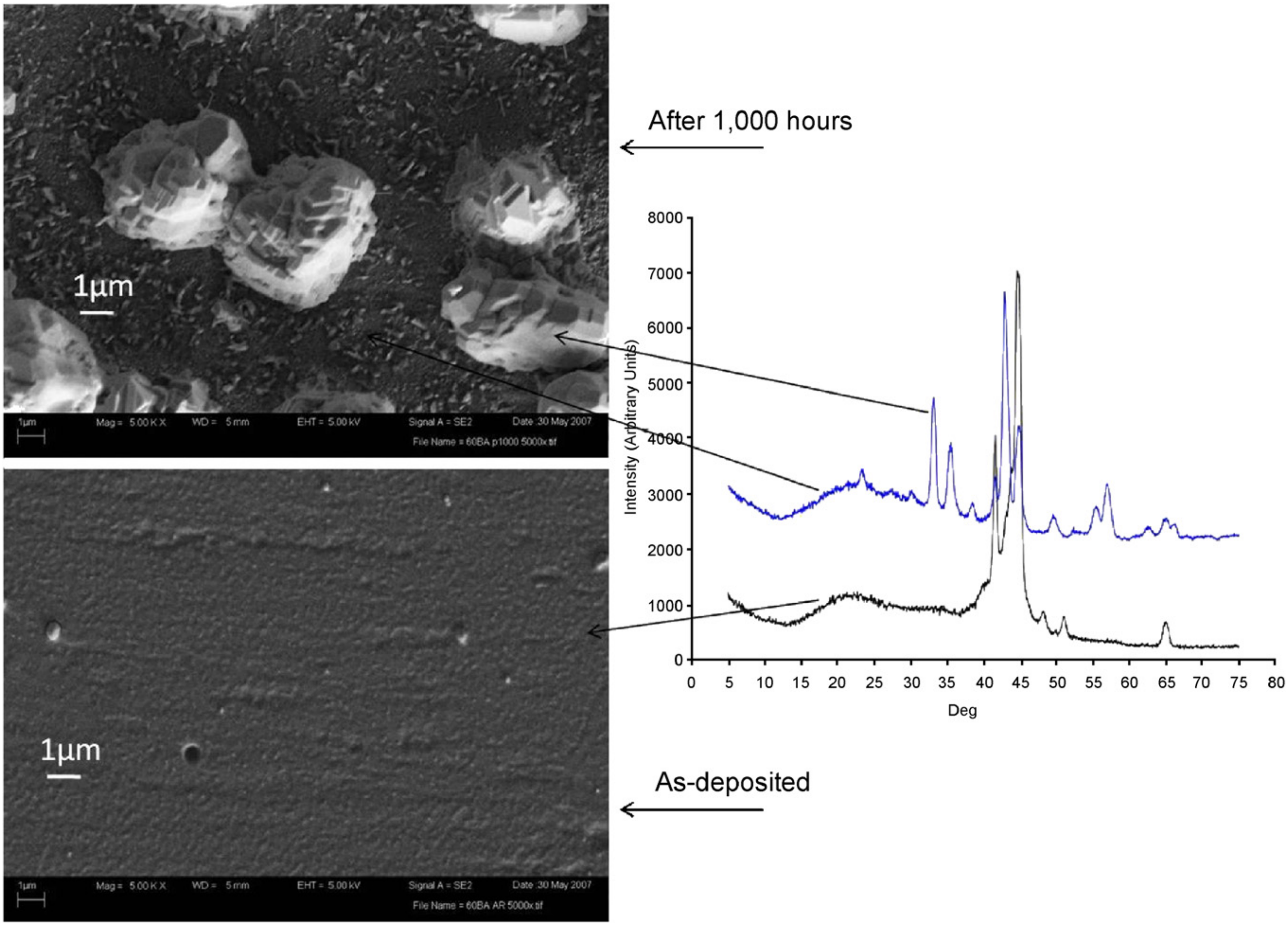

Fig. 7 – SEM images and XRD pattern for coating *γ* before and after 1000 h in 800 °C air.

the amorphous coating contributes a “bump” in the XRD pattern at low angles (e.g., 15–30 °). The surface after exposure exhibits isolated recrystallization (from its weakly crystallized/amorphous as-deposited structure), but remains similar to its original amorphous surface structure in other areas. This phenomenon is also observed in the XRD pattern where the amorphous “bump” remains, but other non-substrate peaks have arisen (presumably due to the localized coating recrystallization). The surface crystallites appear to be complex isomorphic spinel oxides, and are rich in Mn, with the presence of Cr, Ti and Al, e.g. $(\mathrm{Mn,Cr,Ti,Al})_3\mathrm{O}_4$. The amorphous areas between these isolated surface crystallites are relatively rich in Al. An SEM cross-section and EDS elemental map of coating *γ* after 1000 h of ASR testing in 800 °C air is presented in Fig. 8. As with coating *β*, coating *γ* evolved a compositional stratigraphy during the 1000 h exposure. Coating *γ* has appeared to retain its as-deposited thickness (~1.5 µm), with the exception of the isolated and relatively large Mn-rich surface crystallites.

Please cite this article as: Gannon P, et al. Advanced PVD protective coatings for SOFC interconnects. Int J Hydrogen Energy (2008), doi:10.1016/j.ijhydene.2007.12.009

3.2. ASR measurements

Fig. 9 summarizes ASR measurements for the three coatings presented here (Tables 1 and 2) and for uncoated FSS 430. The uncoated FSS 430 exhibits initially low ASR values ($<20\,\text{m}\Omega\,\text{cm}^2$), which increase steadily throughout the test ($>60\,\text{m}\Omega\,\text{cm}^2$ at 1000 h). This increase is attributed to continued growth of the Cr_2O_3-dominant TGO surface layer (in addition to the formation of SiO_2), and alone limits uncoated FSS 430 as an SOFC-IC at 800 °C.

Coating α (at $\sim 2\,\mu\text{m}$) has the highest ASR values, which decrease significantly from the test initiation and stabilize at $\sim 90\,\text{m}\Omega\,\text{cm}^2$ after 1000 h. The observed ASR decrease is attributed to the localized recrystallization of $(Cr,Mn)_3O_4$ resulting from the outward transport of polyvalent Mn from the steel through coating α (presented and discussed above). Initially, the ASR values for coating α and other coatings of similar compositions (not presented here) are very high (often un-measurable for ~100 h); however, as the Mn outward transport pathways develop, the ASR effectively lowers, potentially due to a percolating network of conductive Mn-oxides through the otherwise dielectric amorphous alumina-based coating α.

Coating β began at an initially lower ASR, then decreased slightly and stabilized with time at $\sim 30\,\text{m}\Omega\,\text{cm}^2$ throughout the 1000 h test. The ASR decrease may be due to the effect described above, with Mn outward diffusion increasing the coating conductivity. The lower ASR values (compared with coating α) are likely due to the electronically conductive Co-oxide coating components, which recrystallize to form spinel phases during the exposure period (e.g., $CrCo_2O_4$).

Coating γ has the lowest ASR, which begins low ($<25\,\text{m}\Omega\,\text{cm}^2$) and exhibits relative stability during the 1000 h measurement ($<25\,\text{m}\Omega\,\text{cm}^2$). The as-deposited coating composition (Mn-rich conductive oxides from the LAFAD target (Tables 1 and 2)) appears to exhibit high electronic conductivity (low ASR). The observed stability may be

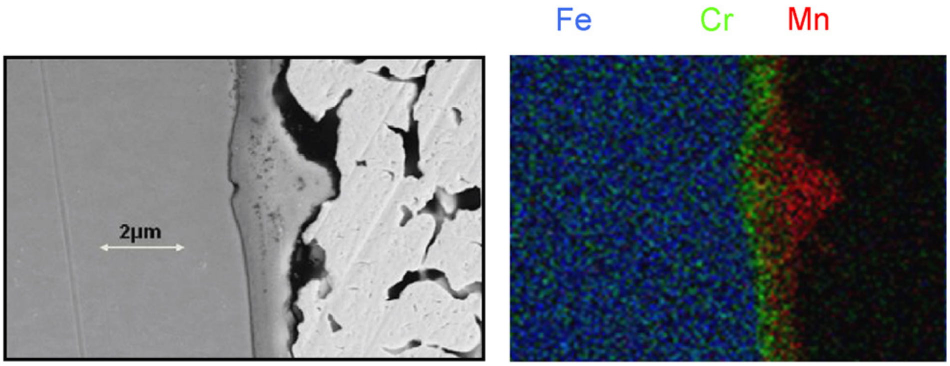

Fig. 8 – SEM cross-section and EDS elemental map of coating γ after 1000 h in 800 °C air.

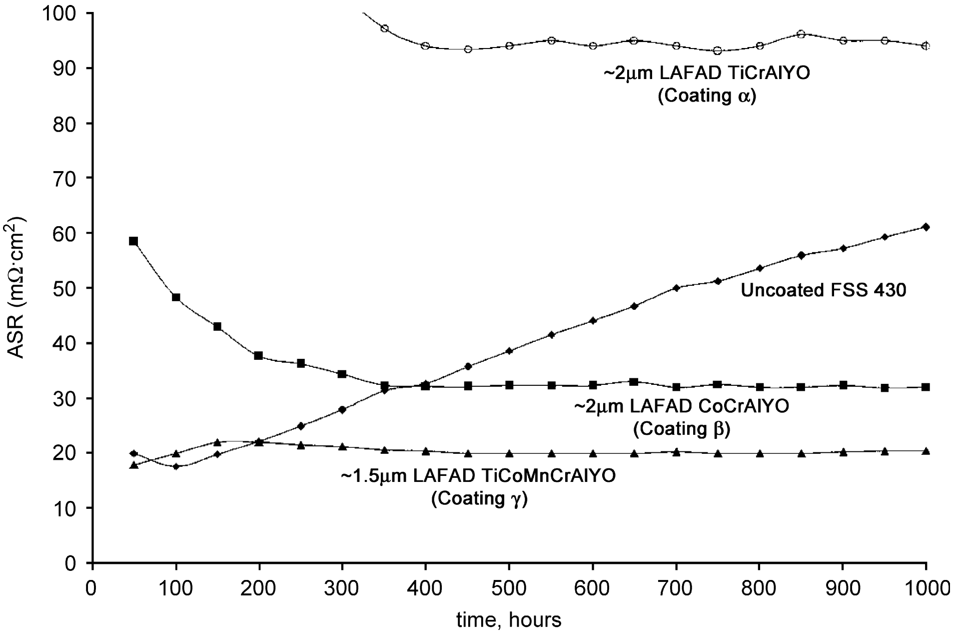

Fig. 9 – Summary of ASR measurements for LAFAD coated and uncoated FSS 430 up to 1000 h in 800 °C air.

Please cite this article as: Gannon P, et al. Advanced PVD protective coatings for SOFC interconnects. Int J Hydrogen Energy (2008), doi:10.1016/j.ijhydene.2007.12.009

afforded to the diffusion-barrier coating components (similar in composition to coating α). During the exposure, isolated surface crystallites (rich in Mn) form and separate the amorphous regions of relatively Al-rich oxides. This combination of coating regions with high conductivity and high transport barrier properties helps explain the observed low and stable ASR values.

To summarize ASR results, LAFAD coatings containing Mn and/or Co as-deposited demonstrate lower ASR values than those without (e.g., coating α). LAFAD coatings without Mn and/or Co as-deposited (e.g., coating α) exhibit higher ASR values, which decrease with increasing time. This phenomenon is attributed to the outward transport of Mn from the steel through the coating, which effectively decreases ASR with time. All LAFAD coatings presented here appear to significantly inhibit the inward transport of oxygen, as evidenced by the observed dimensional stability of the coatings.

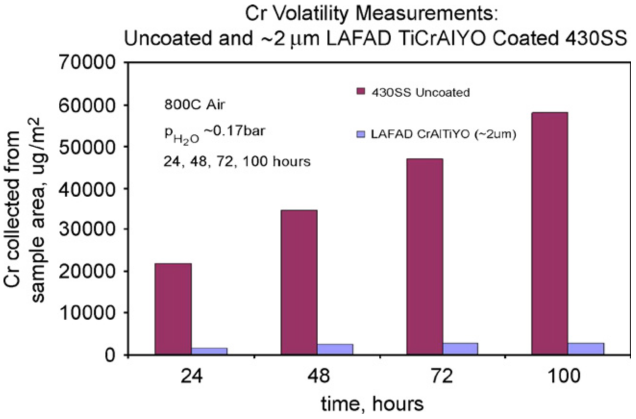

Fig. 10 – Cumulative Cr-volatility measurements from LAFAD coated (coating α) and uncoated FSS 430.

3.3. *Cr-volatility measurements*

Fig. 10 presents Cr-volatility measurements from coated and uncoated FSS 430 specimens (data from a ~2 μm coating α on both sides of FSS 430 is presented). In this case, cumulative, area specific Cr amounts are reported for ~24 h increments up to 100 h. Compared with uncoated FSS 430, substantial Cr-volatility reduction is observed with coating α. Cr volatility for the uncoated 430 continues to increase, transporting $>50,000\,\mu g/m^2$ from the specimen during the 100 h test. This compares with $<3000\,\mu g/m^2$ from the coated specimen, which was not observed to increase between ~72 and 100 h into the test. The atomic percentage of Cr measured in coating 3 is ~14 at%, compared to ~14–40 at% within the duplex TGO layer on uncoated FSS 430SS [22]. Therefore, the reduced total amount of surface Cr (available to form volatile Cr(VI) oxides) in the coating compared to the native TGO scale does not fully explain the observed Cr-volatility reduction. The thermodynamic activity of Cr_2O_3, $a_{Cr_2O_3}$, must be significantly lower within the LAFAD TiCrAlYO coatings compared with the duplex $Cr_2O_3/(Cr,Mn)_3O_4$-based TGO layers formed on the uncoated FSS 430. This has been observed in other Cr-containing oxides, e.g., $LaCrO_3$, where the equilibrium vapor pressures of volatile Cr species are lower than would be predicted on the basis of Cr concentration alone [23].

For complex ceramic oxides lacking thermochemical data (e.g., weakly crystallized/amorphous LAFAD TiCrAlYO coatings) thermodynamic equilibrium modeling of Cr volatility can be approached via considerations of regular solid solutions, in which Gibbs free energy of a multiple component

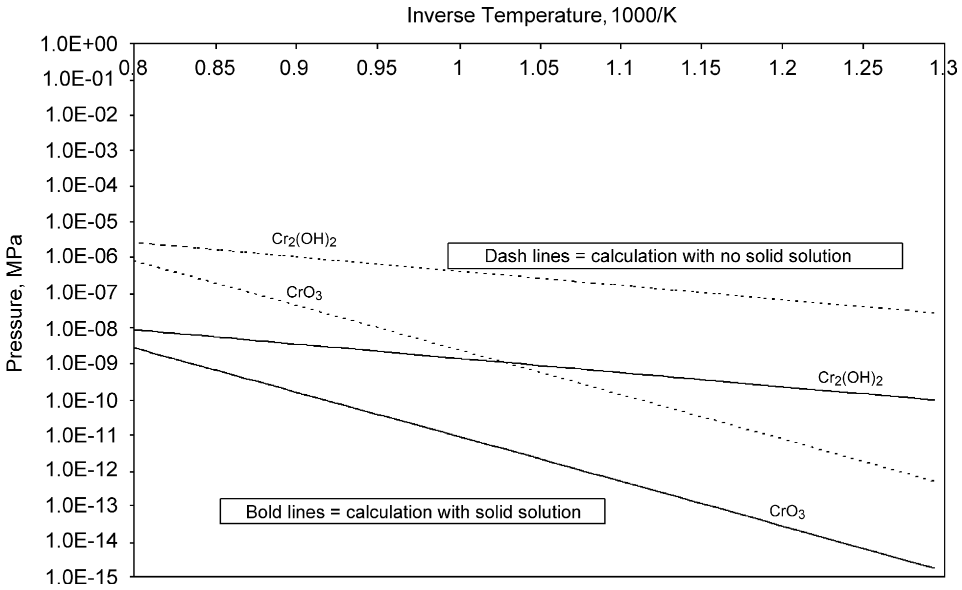

Fig. 11 – Thermodynamic equilibrium vapor pressure models for Cr volatility from coating α composition in moist air with and without ideal solid solutions.

Please cite this article as: Gannon P, et al. Advanced PVD protective coatings for SOFC interconnects. Int J Hydrogen Energy (2008), doi:10.1016/j.ijhydene.2007.12.009

system is lower in an intermixed state compared with that of individual, immiscible components. Results from equilibrium thermodynamic modeling of vapor pressures of predominant Cr-containing gas species (using TERRA and regular solution models) are shown in Fig. 11. A multi-fold reduction in vapor phase Cr species is predicted to exist above a regular solid solution (having the same composition as the TiCrAlYO coating α) vs. the composite case (in which each oxide is immiscible with each other). This could help to explain the dramatic reduction of Cr volatility observed in the Cr-containing LAFAD TiCrAlYO coating. In addition to solid-state Cr transport investigations, Cr-volatility measurements for other Cr-containing coatings are in progress.

4. Future work

Ongoing efforts are to accurately identify the role of each LAFAD coating constituent in high-temperature behavior and to leverage this understanding in future SOFC-IC protective coating designs. For example, the addition of elements which promote formation of conductive oxides, such as Co and/or Mn, appears to significantly reduce ASR values. However, the observed recrystallization of these conductive LAFAD layers may eventually lead to unwanted inward oxygen penetration, and regular, unabated corrosion of the FSS 430 substrate, which may form insulating oxide layers (e.g., SiO_2). Next generation LAFAD SOFC-IC coatings for FSSs will be engineered to combine desirable effects of coating constituents (e.g., the transport-barrier characteristic of the amorphous alumina-based material with sufficient presence of electronically conductive components (e.g., Co and/or Mn oxides)). In addition, experimentation with LAFAD coated FSS 430 specimens in contact with both cathode and seal materials and work toward testing in operational stacks have commenced. The varying requirements of different surfaces on the SOFC-IC may favor the use of patterned coating compositions and/or architectures, all on complex 3-D ICs, making conformity imperative and further investigations into these areas warranted.

5. Summary

Three unique LAFAD MCrAlYO coatings (M = Ti, Co and/or Mn) were deposited on FSS 430 and investigated as a function of SOFC-IC exposures for 1000 h in 800 °C air. The LAFAD coatings exhibited impressive thermal stability and transport-barrier capacities, by virtue of the minimal changes in total coating thickness over the 1000 h oxidative exposure. As-deposited coatings with Co and/or Mn demonstrated low and stable ASR values, yet recrystallized and evolved a compositional stratigraphy during the exposure. Coatings without deposited Co and/or Mn oxides exhibited much higher ASR values, which lowered considerably during the 1000 h test, yet exhibited the highest thermal stability (remaining predominately amorphous) of the three LAFAD coatings during the exposure. Mn from the FSS 430 substrate appeared to effectively transport through all coatings and promote the formation of complex spinel oxide surface crystallites. This occurrence was often observed to be localized and follow rough topological features on the FSS 430 substrate surface (e.g., roll marks).

By combining coating components with different desirable attributes, there is a considerable promise to engineer optimized LAFAD coating compositions for the SOFC(IC) application. LAFAD MCrAlYO coatings show promise for FSS 430 as a SOFC-IC material at ~800 °C. Dramatically improved thermal stability, low and stable ASR values and minimal Cr volatility were observed with coated FSS 430 relative to uncoated FSS 430. Further evaluations of LAFAD ceramic oxide SOFC-IC protective coatings will focus on their thermal cycling stability, as well as diffusion-barrier properties and ASR in contact with SOFC components (both cathodes and sealants).

Acknowledgments

Helpful discussions with Drs. Z. Gary Yang and Jeff Stevenson at Pacific Northwest National Laboratory (PNNL) are kindly acknowledged. Work at MSU was supported through the High-Temperature Electrochemical Center (HiTEC) by a DOI and DOE subcontract from PNNL, number 3917(413060-A). Portions of this work were supported by DOE under contract DE-FC26-04NT42225, and supervised by DOE project manager, Dr. A. Manivannan. Opinions, findings, conclusions or recommendations expressed herein are those of the author(s) and do not necessarily reflect the view of the DOE.

REFERENCES

[1] Singhal SC, Kendall K. High-temperature solid oxide fuel cells: fundamentals design and applications. Amsterdam: Elsevier; 2004.

[2] Minh NQ, Takahashi T. Science and technology of ceramic fuel cells. Amsterdam: Elsevier; 1995.

[3] Fuel Cell Handbook, 7th ed. EG&G Services, Inc., Science Applications International Corporation, DoE, Office of Fossil Energy, National Energy Technology Laboratory; 2004.

[4] Williams M. In: Singhal SC, Yokakawa H, editors. Proceedings of the 7th international symposium on solid oxide fuel cells. Pennington, NJ: The Electrochemical Society Inc.; 2003.

[5] Dhanaraj N, Beuth J, Meier G, Pettit F, Hammer J, Laney S. Interfacial fracture testing to evaluate the durability of SOFC interconnect alloys. In: Materials science and technology—proceedings of the conference, vol. 3, 2005, p. 165–75.

[6] Mikkelsen L, Dinesen AR, Hendriksen PV. Interface resistance between FeCr alloys and La0.85Sr 0.15MnO3. In: 207th meeting of the electrochemical society—meeting abstracts; 2005. p. 1157.

[7] Jiang SP, Zhang S, Zhen YD. Early interaction between Fe–Cr alloy metallic interconnect and Sr-doped $LaMnO_3$ cathodes of solid oxide fuel cells. J Mater Res 2005;20(3):747–58.

[8] Gindorf C, Singheiser L, Hilpert K. Chromium vaporisation from Fe. Cr base alloys used as interconnect in fuel cells, Steel Res 2001;72(11–12):528–33.

[9] Krumpelt M, Cruse T, Terry A, Hash MC. Chromium interactions with cathode materials. In: Proceedings—electrochemical society, v PV 2005-07, solid oxide fuel cells IX, SOFC IX: materials—proceedings of the international symposium; 2005. p. 1578–83.

Please cite this article as: Gannon P, et al. Advanced PVD protective coatings for SOFC interconnects. Int J Hydrogen Energy (2008), doi:10.1016/j.ijhydene.2007.12.009

[10] Tucker MC, Kurokawa H, Jacobson CP, De Jonghe LC, Visco SJ. A fundamental study of chromium deposition on solid oxide fuel cell cathode materials. J Power Sources 2006;160(1):130–8.

[11] Gorokhovsky VI. United States Patent no. 7300559 B2Nov. 27, 2007.

[12] Gorokhovsky VI. Oxidation resistant, Cr-retaining, conductive coatings on metallic interconnects for SOFC interconnects, presented at the 7th annual SECA workshop and peer review, September 12–16, 2006 ⟨ http://www.netl.doe.gov/publications/proceedings/06/seca/pdf/Gorokhovsky.pdf⟩.

[13] Yang ZG, Li X, Singh P, Stevenson JW, Xia G, Zhou X. Development of $(Mn, Co)3O_4$ protection layers on ferritic stainless steels for SOFC interconnect applications. In: TMS annual meeting, materials in clean power systems: applications, corrosion and protection—symposium sponsored by the corrosion and environmental effects committee of the structural materials division (SMD) of the mine; 2006. p. 81–90.

[14] Stanislowski M, Froitzheim J, Niewolak L, Quadakkers WJ, Hilpert K, Markus T, et al. Reduction of chromium vaporization from SOFC interconnectors by highly effective coatings. J Power Sources 2007;164(2):578–89.

[15] Johnson C, Gemmen R, Poston Jr JA, Schaeffer C, Orlovskaya N, Fegely L, et al. Perovskite based protective coatings for solid oxide fuel cell metallic interconnects. In: Proceedings—electrochemical society, v PV 2005-07, solid oxide fuel cells IX, SOFC IX: materials—proceedings of the international symposium; 2005. p. 1842–50.

[16] Chen X, Hou PY, Jacobson CP, Visco SJ, De Jonghe LC. Protective coating on stainless steel interconnect for SOFCs: oxidation kinetics and electrical properties. Solid State Ionics 2005;176(5–6):425–33.

[17] Gorokhovsky VI, Gannon PE, Deibert MC, Smith RJ, Kayani A, Kopczyk M, et al. Deposition and evaluation of protective PVD coatings on ferritic stainless steel SOFC interconnects. J Electrochem Soc 2006;153(10): A1886–93.

[18] Jehn H, Reiners G, Siegel N. DIN-Fachbericht (Special Report) 39, Charakterisierung duenner Schichten (Characterization of thin layers). Berlin: Beuth-Verlag; 1993.

[19] Gannon PE, Tripp CT, Knospe AK, Ramana CV, Deibert M, Smith RJ, et al. High-temperature oxidation resistance and surface electrical conductivity of stainless steels with filtered arc Cr–Al–N multilayer and/or superlattice coatings. Surf Coat Technol 2004;188–189:55–61.

[20] Collins C, Lucas J, Buchanan TL, Kopczyk M, Kayani A, Gannon PE. et al. Chromium volatility of coated and uncoated steel interconnects for SOFCs. Surf Coat Technol 201 (7): 2006; (special issue) 4467–70.

[21] Vatolin NA, Moiseev GK, Trusov BG. Thermodynamic modeling in high temperature inorganic systems, metallurgy, Moscow; 1994 (in Russian).

[22] Yang ZG, Hardy JS, Walker MS, Xia G, Simner SP, Stevenson JW. Structure and conductivity of thermally grown scales on ferritic Fe–Cr–Mn steel for SOFC interconnect applications. J Electrochem Soc 2004;151(11):A1825–31.

[23] Hilpert K, Das D, Miller M, Peck DH, Weiss K K. Chromium vapor species over solid oxide fuel cell interconnect materials and their potential for degradation processes. J Electrochem Soc 1996;143(11):3642–7.